# In vivo detection of microscopic anisotropy using quadruple pulsed-field gradient (qPFG) diffusion MRI on a clinical scanner

Alexandru V. Avram [a,*], Evren Özarslan [a,b], Joelle E. Sarlls [c], Peter J. Basser [a]

[a] Section on Tissue Biophysics and Biomimetics, PPITS, NICHD, National Institutes of Health, Bethesda, MD 20892, USA
[b] Center for Neuroscience and Regenerative Medicine, Uniformed Services University of the Health Sciences, Bethesda, MD 20814, USA
[c] National Institute of Neurological Disorders and Stroke, National Institutes of Health, Bethesda, MD 20892, USA

## ABSTRACT

We report our design and implementation of a quadruple pulsed-field gradient (qPFG) diffusion MRI pulse sequence on a whole-body clinical scanner and demonstrate its ability to non-invasively detect restriction-induced microscopic anisotropy in human brain tissue. The microstructural information measured using qPFG diffusion MRI in white matter complements that provided by diffusion tensor imaging (DTI) and exclusively characterizes diffusion of water trapped in microscopic compartments with unique measures of average cell geometry. We describe the effect of white matter fiber orientation on the expected MR signal and highlight the importance of incorporating such information in the axon diameter measurement using a suitable mathematical framework. Integration of qPFG diffusion-weighted images (DWI) with fiber orientations measured using high-resolution DTI allows the estimation of average axon diameters in the corpus callosum of healthy human volunteers. Maps of inter-hemispheric average axon diameters reveal an anterior–posterior variation in good topographical agreement with anatomical measurements reported in previous post-mortem studies. With further technical refinements and additional clinical validation, qPFG diffusion MRI could provide a quantitative whole-brain histological assessment of white and gray matter, enabling a wide range of neuroimaging applications for improved diagnosis of neurodegenerative pathologies, monitoring neurodevelopmental processes, and mapping brain connectivity.

Published by Elsevier Inc.

## Introduction

Quantifying microanatomical features of neurons, such as mean axon diameters, can provide valuable neuropathological and functional information. Current approaches for quantifying white matter microstructure, however, rely on invasive histological methods such as electron-microscopy. While these morphometric techniques offer excellent spatial resolution, they are prone to bias from dehydration-induced shrinkage during tissue preparation and shearing deformation during slicing (Aboitiz et al., 1992). Above all, biopsy-driven electron microscopy can only sample cells from a few tissue locations within a microscopic field-of-view (FOV) and is not generally available in the clinical setting. Instead, a non-invasive, whole-brain histological assessment of cell features averaged over volumes of a few microliters (a typical MRI voxel size) could provide unprecedented neuroanatomical information of great clinical and scientific significance.

Over the past decade diffusion tensor imaging DTI (Basser et al., 1994) has become the most sensitive clinical tool for non-invasive assessment of white matter microstructural changes (Pierpaoli and Basser, 1996; Pierpaoli et al., 2001) and mapping of brain connectivity (Basser et al., 2000; Mori et al., 1999). The anisotropy of the estimated diffusion tensor (Basser, 1995) reflects the orientation order of the underlying microstructure and is modulated both by the macroscopic arrangement of white matter fibers (ensemble anisotropy) and by restriction-induced microscopic anisotropy. The coupling between these two mechanisms of anisotropy limits the specificity and selectivity of DTI, making it difficult to correlate observed changes in DTI-derived parameters, *e.g.*, the fractional anisotropy (FA) and the mean apparent diffusion coefficient (ADC) with neuronal specific pathophysiology. For example, decrease in myelination or axon density, edema, or extracellular matrix degradation can all produce the same decrease in diffusion anisotropy measures like FA (Beaulieu, 2002; Pierpaoli and Basser, 1996). A diffusion MRI method that is more specific to microanatomical changes is needed to improve MR assessments in white matter.

Advanced diffusion MRI techniques such as CHARMED (Assaf and Basser, 2005) and AxCaliber (Assaf et al., 2008) MRI can provide estimates of average axon diameters, and diameter distributions, respectively, by acquiring *q*-space (Callaghan et al., 1988) data using the classical single pulsed-field gradient (PFG) diffusion MR measurement (Stejskal and Tanner, 1965) with different diffusion times and

* Corresponding author at: *Eunice Kennedy Shriver* National Institute of Child Health and Human Development, National Institutes of Health, Building 13, Room 3W16, 13 South Drive, Bethesda, MD 20814, USA. Fax: +1 301 435 5035.
*E-mail address:* alexandru.avram@nih.gov (A.V. Avram).

large diffusion weightings. Measuring the size of human brain axons with diameter $d$ of a few micrometers (Aboitiz et al., 1992) requires $q$-values (i.e., $q = (2\pi)^{-1}\gamma\delta_{1,2}G$) on the order of $1/d$ leading to large signal attenuations. To achieve such large $q$-values on whole-body MRI scanners, with maximum gradient strength limited by patient safety (i.e., to prevent peripheral nerve stimulation) and high manufacturing cost, long echo times are necessary. The implicit sensitivity loss due to transverse ($T_2$) magnetic relaxation challenges the feasibility of such single PFG MRI methods for in vivo applications on clinical MRI systems.

An extension of the Stejskal–Tanner single PFG sequence is the multiple PFG (mPFG) MR sequence (also known as multiple-wave-vector diffusion weighted MR) achieved by applying multiple diffusion encoding gradient pairs, or blocks (Cory et al., 1990) with varying orientations and a variable time separation (Fig. 1A). The mPFG diffusion MR experiment (Ozarslan and Basser, 2007) quantifies the correlation of water motions during consecutive diffusion blocks, thereby exclusively characterizing diffusion of water in restricted compartments (microscopic anisotropy) and providing a direct measure of average cell features (e.g., mean axon diameter in white matter). The simplest implementation of mPFG MR, double PFG (dPFG) MR, uses two blocks of diffusion sensitizing gradient pairs $G_1$ and $G_2$ with pulse durations $\delta_1$ and $\delta_2$ separated by mixing time $\tau_m$, and oriented at an angle $\psi$ relative to each other. If both gradient pairs are applied in a plane orthogonal to the white matter fiber orientation, in the limit of short $\tau_m \ll D/d$ the angular $\psi$-dependence of the diffusion attenuation can furnish an estimate of the average axon diameter (Eq. (1)). Double PFG diffusion MRI theory and methodology have been extensively validated in both non-biological (Komlosh et al., 2011; Shemesh and Cohen, 2011) and biological samples (Koch and Finsterbusch, 2008; Lawrenz and Finsterbusch, 2011; Shemesh et al., 2011b), including gray and white matter (Komlosh et al., 2007;

Shemesh et al., 2011a). Recently, the ability to measure average axon diameters in white matter using dPFG diffusion MRI has been validated with histology (Komlosh et al., 2012). Although in vitro studies on both MR microimaging and whole-body MRI systems (Koch and Finsterbusch, 2008; Lawrenz and Finsterbusch, 2011) provide good agreement with theory, the translation of this research to in vivo human applications remains challenging (Koch and Finsterbusch, 2011). Preliminary results support the feasibility of double PFG MRI for clinical applications on whole-body MRI scanners, but underscore the need for improved white matter sensitivity and numerical modeling methods (Koch and Finsterbusch, 2011).

Given the limited gradient strength available even on today's state-of-the-art whole-body MRI scanners, the large diffusion attenuations required for detection of axon diameters on the order of a few micrometers can only be achieved using diffusion gradient pulses of longer durations, resulting in longer echo times (TE) and implicitly poor white matter signal-to-noise ratio (SNR). However, theoretical predictions indicate that concatenating several double PFG blocks can significantly increase the sensitivity of mPFG diffusion MRI to smaller cell diameters and improve its applicability on clinical scanners (Finsterbusch, 2009, 2010). In particular, for an experiment with $n$ concatenated double PFG blocks using $|\mathbf{q_1}| = |\mathbf{q_2}| = q$ and infinitesimally short diffusion gradient pulse durations ($\delta \rightarrow 0, \Delta \rightarrow \infty$), the theoretical diffusion signal attenuation as a function of the angle $\psi$ between $\mathbf{q_1}$ and $\mathbf{q_2}$ can be approximated analytically at short mixing time $\tau_m \rightarrow 0$ (Finsterbusch, 2009):

$$E_0(\psi) = 1 - 8n\pi^2 q^2 \langle A \rangle_{iso} - (2n-1)4\pi^2 q^2 \langle A \rangle_{iso}\cos\psi \qquad (1)$$

where $\langle A \rangle_{iso}$ is the mean-squared radius of gyration reflecting average cell size and shape characteristics (Ozarslan, 2009). The diffusion signal attenuation $E_0(\psi)$ exhibits an angular $\psi$-modulation with
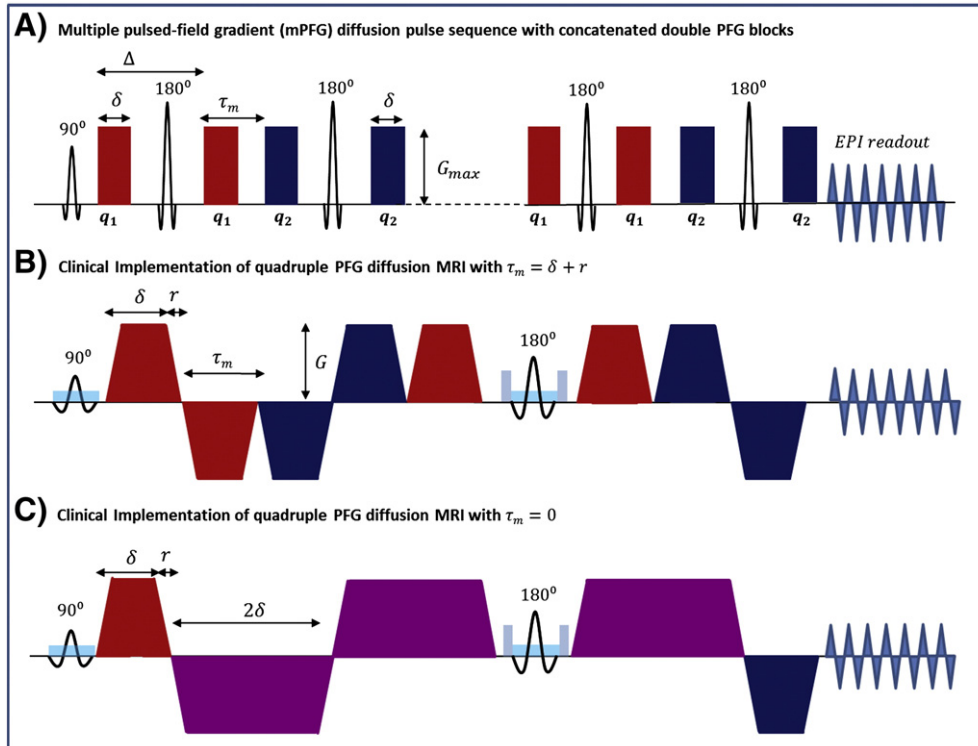


**Fig. 1.** A. Pulse sequence schematic diagram for multiple pulsed-field gradients (mPFG) spin echo diffusion MRI with concatenated double PFG blocks in the theoretical short gradient pulse limit ($\delta \rightarrow 0, \Delta \rightarrow \infty$). The signal is analyzed as a function of the angle $\psi$ between the two diffusion wave vectors $\mathbf{q_1}$ (red) and $\mathbf{q_2}$ (blue). B. Schematic diagram of our clinical slice-selective quadruple pulsed-field gradient (qPFG) spin echo diffusion MRI sequence with EPI readout and $\tau_m = \delta + r = 13.4$ ms, where $\delta = 12.6$ ms and $r = 0.8$ ms are the pulse width (including ramp-up and plateau durations) and ramp-down time for all diffusion gradient pulses. C. Schematic diagram of our clinical slice-selective qPFG diffusion MRI pulse sequence with short $\tau_m = 0$ ms. Gradient pulses in consecutive diffusion encoding blocks are fused into a single pulse (purple) with width $2\delta$ and amplitude $(\mathbf{G_1} + \mathbf{G_2})/2$, corresponding to $\mathbf{q_1} + \mathbf{q_2}$. (For interpretation of the references to color in this figure legend, the reader is referred to the web version of this article.)

amplitude $(2n-1)\gamma^2\delta^2G^2\langle A\rangle_{iso}$ reflecting anisotropy exclusively due to microscopic restrictions. For larger number $n$ of concatenated double PFG blocks, this modulation amplitude increases resulting in improved sensitivity to smaller axon diameters. The $q$-value can then be reduced slightly to limit overall diffusion signal attenuation $1 - E_0(\psi)$ (i.e. reduce total $b$-value) and achieve optimal contrast-to-noise ratio.

In this study, we translate the mPFG NMR methodology to a clinical MRI scanner and assess its potential for clinical applications. We design a quadruple pulsed-field gradient (qPFG) spin echo (SE) diffusion MRI pulse sequence and demonstrate that, within the constraints of conventional gradient hardware available on whole-body MRI scanners, it is possible to detect restriction-induced microscopic anisotropy in individual voxels. We employ a recently developed mathematical framework (Ozarslan et al., 2009) to incorporate intra-voxel fiber orientations measured with high-resolution DTI and estimate average axon diameters of inter-hemispheric fiber pathways in the corpus callosum. The ability to conduct mPFG diffusion MRI experiments *in vivo* using standard gradient hardware available on clinical MRI scanners could have an immediate impact on our ability to investigate many brain pathologies.

## Methods

Following the model employed in the CHARMED framework (Assaf and Basser, 2005), we consider that myelinated axons in human white matter can be conveniently approximated by infinitely-long parallel cylinders with impermeable boundaries surrounded by hindered extracellular water. The diffusion signal attenuation $E(\psi)$ in an mPFG MRI experiment (Fig. 1A) with $n$ concatenated dPFG diffusion blocks ($\mathbf{q_1}$ and $\mathbf{q_2}$) can be expressed as the weighted sum of contributions from water trapped within cylindrical myelinated axons $E^{ax}(\psi)$ and unrestricted extracellular water $E^{out}(\psi)$:

$$E(\psi) = f\ E^{ax}(\psi) + (1-f)E^{out}(\psi) \qquad (2)$$

where the signal fraction $f$ incorporates contributions from both proton density and $T_2$ relaxation. Analytical expressions such as Eq. (1) can be used to approximate $E^{ax}(\psi)$ under certain conditions: $\delta \to 0$, $\Delta \to \infty$, $\tau_m \to 0$ or $\tau_m \to \infty$. Due to limited gradient strength, these assumptions generally break down on clinical MRI scanners and Eq. (1) provides only a qualitative description of the mPFG diffusion attenuation.
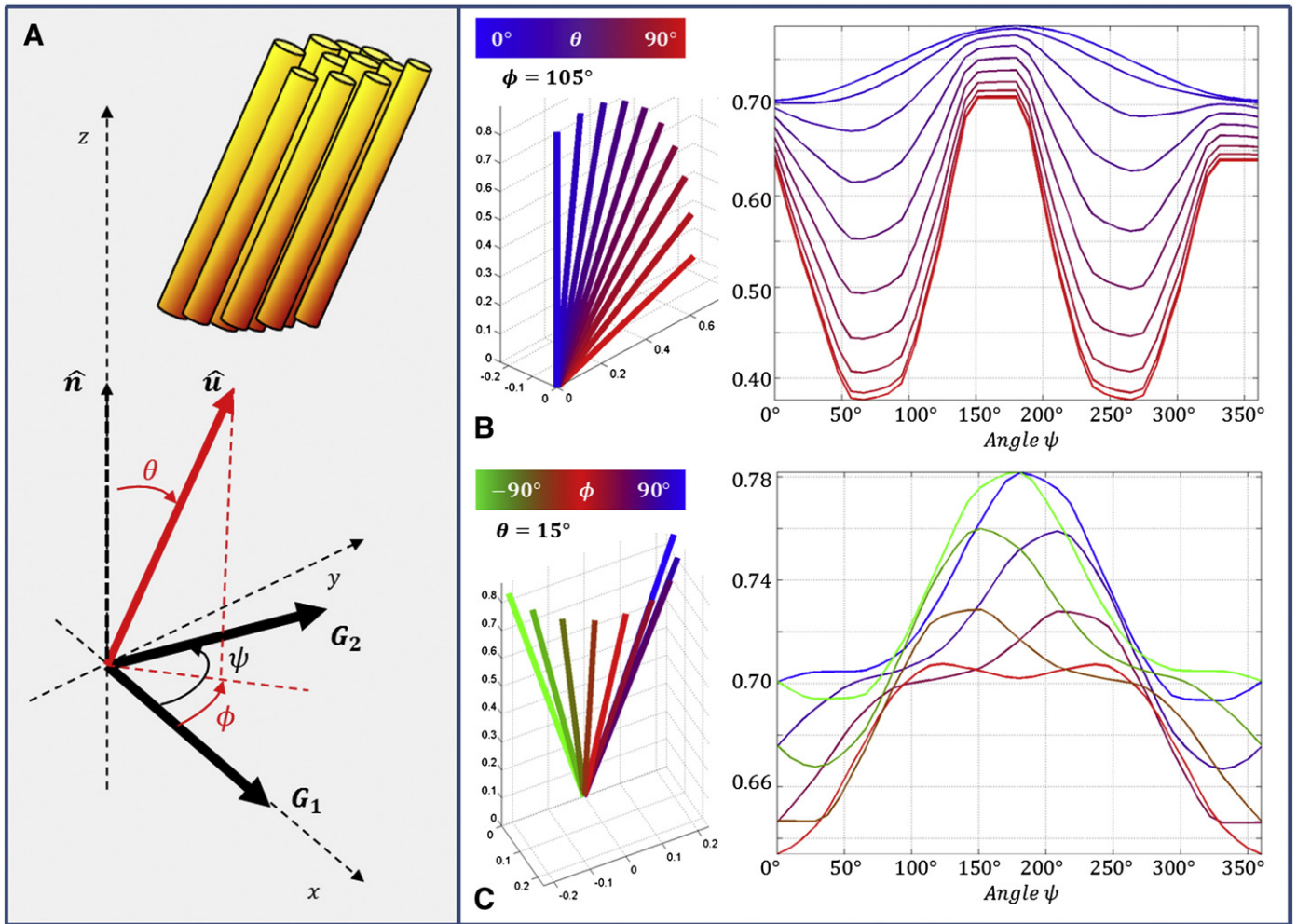


**Fig. 2.** A. The fiber orientation $\hat{u}$ is defined by spherical coordinates $\theta$ (polar angle) and $\phi$ (azimuthal angle) with respect to the normal $\hat{n}$ to the plane of the applied diffusion gradients $\mathbf{G_1}$ and $\mathbf{G_2}$. Both diffusion gradients are applied in the $xy$-plane with $\mathbf{G_1}$ aligned along the $x$-axis and $\mathbf{G_2}$ at an angle $\psi$ relative to $\mathbf{G_1}$. Angular qPFG diffusion attenuation profiles $E^{ax}(\psi)$ were evaluated numerically using the multiple correlation function formalism (Ozarslan et al., 2009) for the pulse sequences shown in Figs. 1B and C with maximum gradient strength of 50 mT/m/axis, intra-axonal diffusivity D = 1.5 μm²/m and an axon diameter $d = 5$ μm. B. For a fixed azimuthal angle (e.g., $\phi = 105°$), as the inclination $\theta$ increases coupling of macroscopic (ensemble) anisotropy can generate large signal minima significantly changing the shape of the sinusoidal profile. For $\phi \neq 90°$, 270°, the amplitude of the main peak is reduced and the position shifted away from $\psi = 180°$ rendering the profile asymmetric. C. Even for small polar angles (e.g., $\theta = 15°$), the shape of $E^{ax}(\psi)$ is very sensitively dependent on variations in $\phi$, (i.e., fiber orientation with respect to $\mathbf{G_1}$). This dependence increases at larger inclinations as macroscopic and microscopic anisotropies become more strongly coupled.

Characterizing the mPFG signal $E^{ax}(\psi)$ quantitatively for arbitrary parameters ($\delta$, $\Delta$, and $\tau_m$) requires a powerful mathematical framework capable of accounting for finite ramps, widths, orientation and timing parameters of all gradient pulses (Ozarslan and Basser, 2008). Assuming Gaussian diffusion for extracellular water, the evaluation of $E^{out}(\psi)$ can be achieved through numerical integration of exact gradient pulse waveforms (Basser et al., 1994; Stejskal and Tanner, 1965):

$$E^{out}(\psi) = \exp\left[-\gamma^2 \int_0^T \left(\int_0^t \boldsymbol{G}(t')dt'\right) \cdot \boldsymbol{D}\left(\int_0^t \boldsymbol{G}(t')dt'\right)dt\right]. \quad (3)$$

When both gradients $\boldsymbol{G_1}, \boldsymbol{G_2}$ are applied orthogonal to the fiber orientation, the average axon diameter can be estimated using Eq. (2). However, deviations of the fiber orientation $\hat{u}$ with respect to the normal $\hat{n}$ to the ($\boldsymbol{G_1}, \boldsymbol{G_2}$)-plane of the applied gradient pulses can generate strong coupling between microscopic and macroscopic anisotropies, making the extraction of microscopic anisotropy problematic. It is then necessary to use additional information (Ozarslan et al., 2011) such as mPFG DWIs acquired with a full 3D diffusion encoding scheme, or estimates of fiber orientations measured with a separate single-PFG (e.g. DTI) scan.

Numerous studies have investigated the theoretical dependence of the mPFG diffusion signal attenuation on sequence parameters and microstructural properties such as diffusivity, compartment shape, size, and orientation distributions (Ozarslan, 2009). The development of the multiple correlation functions framework (Grebenkov, 2007; Ozarslan et al., 2009) based on the Laplacian eigenvalue formalism proposed by Grebenkov (2007) has enabled efficient numerical evaluation of NMR diffusion signals in systems with simple pore geometries and arbitrary orientations. We employ these recent advances to numerically evaluate the expected diffusion attenuation $E(\psi)$ accounting for exact gradient pulses and fiber orientation $\hat{u}$. We use the multiple correlation functions framework (i.e., Eq. 40 in Ozarslan, 2009) and Eq. (3) to numerically calculate $E^{ax}(\psi)$ and $E^{out}(\psi)$ respectively for different mPFG MRI pulse sequence designs.

*Pulse sequence design and implementation*

Assuming mean diffusivities (Pierpaoli et al., 1996) and axonal diameters (Aboitiz et al., 1992) within the physiological ranges reported in the literature, we investigate the theoretical $\psi$-dependence of white matter diffusion signal attenuation for double PFG and quadruple PFG ($n=2$) pulse sequence designs optimized for use on whole body clinical MRI scanners equipped with a standard gradient hardware (maximum gradient amplitude $G_{max} = 50$ mT/m/axis; slew rate $SR = 200$ T/m/s). To assess sensitivity to small axon diameters of our tentative mPFG MRI clinical pulse sequence designs, we calculated theoretical angular $\psi$-modulation curves $E^{ax}(\psi)$ in experiments with $G_1$ and $G_2$ applied in a plane orthogonal to the fibers' direction, $\hat{u}$, for axon diameters in the range of 1–10 μm and intra-axonal diffusivity $D = 1.5$ μm$^2$/ms.

We implemented a quadruple PFG (qPFG) MRI pulse sequence with single-shot echo-planar imaging (EPI) readout and parallel imaging acquisition (Pruessmann et al., 1999) (Figs. 1B,C). When the diffusion encoding blocks are set to $\boldsymbol{q_1} = \boldsymbol{q_3}$ (Fig. 1B red gradients) and $\boldsymbol{q_2} = \boldsymbol{q_4}$ (Fig. 1B blue gradients), a concatenated dPFG diffusion pulse sequence with $n=2$ is obtained. To maximize the time available for diffusion encoding, bipolar diffusion gradient pulses (Fig. 1B) were used in conjunction with a conventional spin–echo sequence employing a single
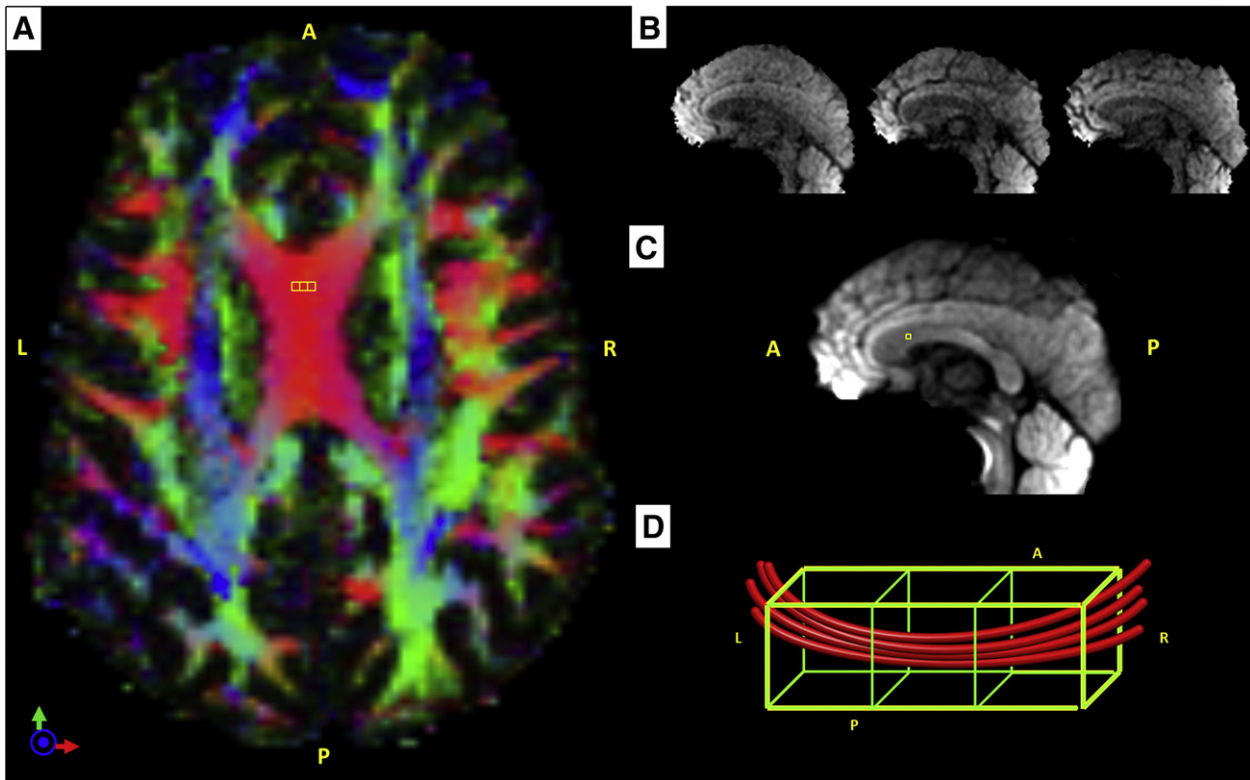


**Fig. 3.** Integration of high-resolution diffusion tensor imaging (DTI) with quadruple pulsed-field gradient (qPFG) diffusion MRI data to account for intravoxel variations in fiber orientation. A. Axial view of directionally encoded color (DEC) maps obtained with 2 mm isotropic DTI in a representative healthy volunteer. B. Diffusion weighted images (DWIs) acquired with 2×2×2 mm$^3$ resolution from three contiguous sagittal DTI slices corresponding to the 6 mm-thick qPFG MR slice shown below. C. Sagittal qPFG DWIs acquired with 2×2×6 mm$^3$ resolution corresponding to the three high resolution DTI slices shown in B. D. Schematic representation of local white matter fiber orientation in a 2×2×6 mm$^3$ qPFG MRI voxel and the three corresponding 2 mm isotropic DTI sub-voxels. Alignment of the qPFG MRI voxel with the underlying fiber orientation minimizes the number of axons contributing to the diffusion signal and allows effective average axon diameter estimation by incorporating intravoxel fiber orientations derived from a separate high-resolution DTI scan (Eq. (4)).

180° refocusing radiofrequency (RF) pulse (Koch and Finsterbusch, 2011). The pulse sequence design was optimized for minimum mixing time $\tau_m = \delta + r$ (where $r$ represents the ramp-down time and $\delta$ denotes pulse width including ramp-up and plateau durations of the trapezoidal gradient pulse) that allows the use of full gradient strength for all diffusion gradient pulses. With the 180° RF refocusing pulse placed between the gradients of the third diffusion pair, our qPFG sequence design in Fig. 1B conveniently accommodates a full k-space EPI readout while keeping $TE < 150$ ms and $\tau_m = \delta + r < 15$ ms. To measure diameters of myelinated axons in white matter (Komlosh et al., 2012), diffusion blocks are applied in a plane orthogonal to the fiber orientation with varying angles $\psi$ between $\mathbf{q_1}$ and $\mathbf{q_2}$. At short $\tau_m = \delta + r$, the correlated motions of water molecules diffusing in microscopic restrictions give rise to a sinusoidal modulation of the intra-axonal signal profile $E^{ax}(\psi)$, peaking at $\psi = 180°$ (Eq. (1)), from which the average axon diameter can be estimated (Ozarslan, 2009). On the other hand, motion of unrestricted extracellular water is uncorrelated during consecutive diffusion blocks leading to no angular dependence of $E^{out}(\psi)$ (Eq. (3)).

Without changing TE, it is possible to fuse gradient pulses from consecutive diffusion blocks into a single gradient pulse corresponding to $\mathbf{q_1} + \mathbf{q_2}$, thereby obtaining a measurement with zero $\tau_m$ (Fig. 1C). Consecutive diffusion gradient pulses with areas $\delta \mathbf{G_1}$ and $\delta \mathbf{G_2}$ can be combined into a trapezoidal pulse with duration $2\delta$ and amplitude given by the vector average $(\mathbf{G_1} + \mathbf{G_2})/2$. This solution makes efficient use of clinical gradients' strength and slew rates, enabling the large $q$-values achieved using maximum gradient amplitude for $\mathbf{G_1}$ and $\mathbf{G_2}$ in the $\tau_m = \delta + r$ sequence (Fig. 1B) to be applied for motion correlation experiments with $\tau_m = 0$. The restricted intra-axonal diffusion signal $E^{ax}(\psi)$ exhibits a larger positive modulation compared to the case with non-zero $\tau_m = \delta + r$, resulting in increased sensitivity to microscopic anisotropy. However, the finite durations of the diffusion gradient pulses generate a $\psi$-dependent b-value with a minimum at $\psi = 180°$ (Eq. (3)) resulting in a negative angular modulation even for the unrestricted extracellular water signal $E^{ex}(\psi)$. This behavior for unrestricted diffusion is not predicted in the "short gradient pulse" approximation and underscores the need for numerical methods in evaluating and fitting mPFG diffusion signal attenuation profiles. To characterize the extent to which the extracellular water can affect the angular profile modulation amplitude we generated theoretical angular qPFG diffusion attenuation curves for experiments with $\tau_m = 13.4$ ms and $\tau_m = 0$ ms assuming different intra-axonal signal fractions (see Supplementary Material).

Finally, we analyzed the effect of fiber orientation misalignment on the expected qPFG diffusion signal attenuation as a function of inclination $\theta$ and azimuthal $\phi$ deviations from the normal to the plane determined by $\mathbf{q_1}$ and $\mathbf{q_2}$ (Fig. 2A). All numerical methods were implemented in MATLAB (Mathworks Inc., Natick, MA, USA) using the multiple correlation function formalism (Ozarslan et al., 2009) and Eq. (3) to evaluate the diffusion signal attenuation profiles.

*Phantom validation*

To quantitatively validate our qPFG MRI sequences and to assess the image distortions due to gradient-induced eddy currents and image acquisition, we conducted a control experiment using a calibrated free diffusion phantom of 35% Polyvinylpyrrolidone (PVP) polymer solution with nominal water diffusivity of $D = 0.81$ μm²/ms similar to human brain tissue (Pierpaoli et al., 2009). Previous diffusion MRI studies using the PVP polymer solution found a monoexponential decay with a mean diffusivity independent of diffusion time, indicating the presence of a single spin population with unrestricted Gaussian diffusion characteristics (Pierpaoli et al., 2009). The phantom was scanned using our novel qPFG diffusion MRI sequences (Figs. 1B and C) with TE/TR = 147/6000 ms, $G_{max} = 50$ mT/m, $\delta = 12.6$ ms, $r = 0.8$ ms, $4q = 1100$ cm⁻¹, 12 angles $\psi$ equally spaced from 0 to $2\pi$, $\tau_m = 13.4$ ms and $\tau_m = 0$ ms, respectively. Sagittal images were acquired with a $96 \times 96$ matrix on a $20 \times 20$ cm² field-of-view (FOV) and 6 mm slice thickness using a single-shot EPI readout with SENSE acceleration factor 2. The total b-value for the experiment was 1200 s/mm². The empirical diffusivity of the phantom was measured in a separate experiment using conventional single PFG diffusion MRI with 6 b-values ranging from 300 to 3000 s/mm². Subsequently, the measured diffusivity was used to calculate the expected qPFG angular profiles for both $\tau_m = 13.4$ ms and $\tau_m = 0$ ms by numerically integrating the exact pulse sequence gradient waveforms using Eq. (3). Finally, the calculated angular qPFG diffusion profiles were compared to those measured using our qPFG MRI pulse sequence.

*In vivo human data*

Data were acquired with the qPFG MRI sequence on four healthy volunteers who provided informed consent in accordance with a research protocol approved by the Institution Review Board. All
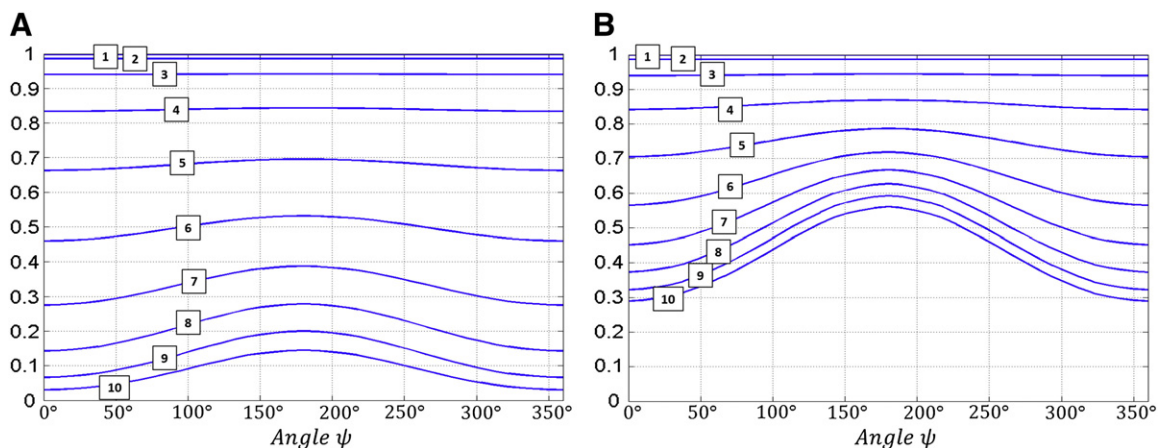


**Fig. 4.** Theoretical comparison of axon diameter sensitivity for clinical multiple pulsed-field gradient (mPFG) diffusion MRI pulse sequences. Angular diffusion signal attenuation profiles $E^{ax}(\psi)$ are numerically calculated (Ozarslan et al., 2009) for both double PFG (A) and quadruple PFG (B) pulse sequence designs, assuming axon diameters from 1 to 10 μm, intra-axonal diffusivity of 1.5 μm²/ms, and mixing time $\tau_m = 0$ ms. Diffusion gradient pulse durations $\delta = 22.6$ ms and $\delta = 12.6$ ms were used for the dPFG and qPFG sequences, respectively. The results qualitatively reflect the behavior predicted analytically by Eq. (1) in the short-pulse limit ($\delta \to 0$, $\Delta \to \infty$). Compared to the dPFG sequence, the qPFG implementation uses lower overall diffusion attenuations and is more sensitive to axon diameter ranges previously reported in the corpus callosum, leading to improved contrast-to-noise ratio (CNR).

experiments were conducted on a 3 T MRI scanner equipped with 50 mT/m/axis gradients, using a 32-channel head RF coil and single-shot EPI with SENSE acceleration factor 2. A spatial spectral excitation pulse was used to avoid contaminations from chemical shift (*i.e.*, fat) (Meyer et al., 1990; Zur, 2000). To prevent confounds due to physiological motion (*e.g.*, blood flow, pulsatile ventricle motion, *etc.*) the qPFG MRI acquisition was cardiac gated using peripheral gating with a 15 ms trigger delay. A repetition time (TR) of 7 R-to-R intervals was sufficient to accommodate full recovery of white matter longitudinal magnetization even in the presence of moderate heart rate fluctuations. Seven contiguous sagittal slices (6 mm slice thickness) were prescribed medially through the center of the corpus callosum and images with $2 \times 2$ mm$^2$ in-plane resolution were acquired in an interleaved fashion, with $TE = 147$ ms. Because the corpus callosum contains tightly packed, highly organized parallel fibers, a mid-sagittal prescription was chosen to maximize the intra-voxel fiber coherence. Diffusion wave vectors $\mathbf{q_1}$ and $\mathbf{q_2}$ were applied in the plane perpendicular to the slice direction with $\delta = 12.6$ ms, $r = 0.8$ ms, and 12 angles $\psi$ equally spaced from 0 to 360°. To mitigate off-resonance induced image distortions due to magnetic field inhomogeneities and/or variations in tissue magnetic susceptibilities, the readout duration was reduced with parallel imaging. Images were acquired with $\tau_m$ alternating between 13.4 ms and 0 ms, four averages for each, for a total scan duration of approximately 15 min. To account for intra-voxel fiber orientation distributions in the $2 \times 2 \times 6$ mm$^3$ qPFG MRI data, we obtained a co-registered high-resolution $2 \times 2 \times 2$ mm$^3$ DTI scan (Sarlls et al., 2011) with $TE/TR = 80/12,000$ ms, 70 non-collinear diffusion directions (10 *b*-values of 300 s/mm$^2$ and 60 *b*-values of 1100 s/mm$^2$) using the same mid-sagittal scan prescription and in-plane resolution as the qPFG MRI scan but three-times smaller slice thickness, 2 mm (Fig. 3). DTI was acquired over the entire brain with a total of 81 slices to allow tracking of inter-hemispheric white matter fibers. Finally a high-resolution $1 \times 1 \times 1$ mm$^3$ T$_2$-weighted fast spin echo (FSE) MRI was obtained to enable accurate registration of both qPFG MRI and DTI datasets to a common structural template.

*Estimating average axon diameters in inter-hemispheric white matter pathways*

The qPFG diffusion MRI and DTI datasets were processed using the TORTOISE pipeline (Pierpaoli et al., 2010). All DWIs were corrected for subject motion and eddy-current distortions, followed by registration to anatomical template. From the high-resolution DTI data, diffusion tensors were calculated using non-linear least square fitting in TORTOISE to obtain maps of FA, axial and mean diffusivities, and principal diffusion direction with 2 mm isotropic resolution.

In each $2 \times 2 \times 6$ mm$^3$ voxel, the mPFG diffusion signal attenuation $E(\psi)$ was modeled as a summation of restricted (intra-axonal) and hindered (extracellular) diffusion signal components ($E_k^{ax}(\psi)$ and $E_k^{out}(\psi)$, respectively) corresponding to three 2 mm isotropic sub-voxels ($k = 1,2,3$), for which high resolution DTI data was acquired (Fig. 3). To account for variations in fiber orientation within the qPFG MRI voxel, the DTI-derived principal diffusion directions $\mathbf{u_k}$ were used as the underlying fiber orientations in each sub-voxel. The number of unknowns in the model was further reduced by approximating the diffusivity of the intra- and extra-cellular compartments ($D_k$, and $D_{k,0}$, respectively) with the apparent axial and mean diffusivities measured in the corresponding sub-voxels with high-resolution DTI. The apparent axial diffusivity quantifies unrestricted diffusion along the direction of the axon and, in regions of coherent tightly-packed fibers such as the human corpus callosum, is determined primarily by intra-axonal diffusivity. Meanwhile, *in vivo* studies that fit similar models for myelinated axons to large single-PFG diffusion datasets while treating the extracellular diffusivity as an unknown model parameter report diffusivity values for the hindered (extracellular) compartment that are similar to mean apparent diffusivities measured with DTI (Barazany et al., 2009). In the absence of a gold standard for measuring intrinsic compartmental diffusivities, these approximations can be used to significantly improve the convergence of the nonlinear fit to the qPFG diffusion measurements. Finally, the alignment of the anisotropic qPFG MRI voxel to the white matter fiber direction maximizes orientational coherence of axons contributing to the diffusion signal and validates the assumptions that average axon diameters $d$ and relative signal fractions $f$ are constant in the three corresponding sub-voxels. With these assumptions, the total diffusion signal attenuation $E(\psi)$ can be written as a summation of Eq. (2) over three sub-voxels:

$$E(\psi) = f\left[\sum_{k=1}^{3} E_k^{ax}(\psi, u_k, D_k, d)\right] + (1-f)\left[\sum_{k=1}^{3} E_k^{out}\left(\psi, D_{k,0}\right)\right]. \qquad (4)$$
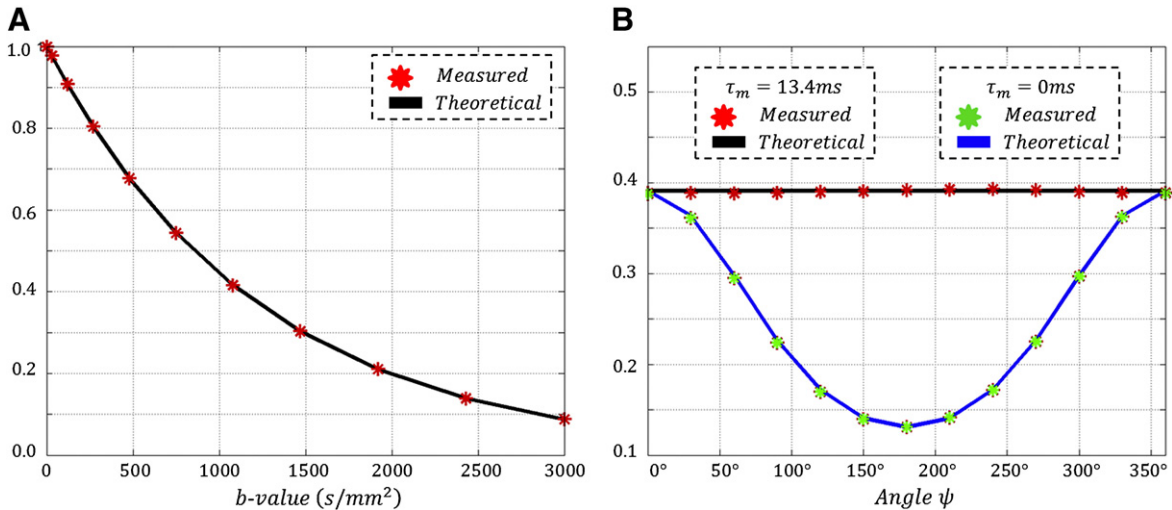


**Fig. 5.** Validation of our quadruple pulsed-field gradient (qPFG) diffusion MRI clinical sequences (Figs. 1B,C) using a calibrated polymer phantom for free diffusion. A Single PFG diffusion signal attenuation measurements (red) as a function of *b*-value were fit with a mono-exponential decay function (black curve) to obtain a diffusivity of $D = 0.81$ μm$^2$/ms. B. The diffusivity measured using the single PFG experiments was used to numerically generate qPFG diffusion signal attenuation profiles $E(\psi)$ for our clinical sequences with $\tau_m = 13.4$ ms (black curve) and $\tau_m = 0.4$ ms (blue curve). These theoretical profiles are in excellent agreement with measured qPFG diffusion attenuations using the same sequence parameters. (For interpretation of the references to color in this figure legend, the reader is referred to the web version of this article.)

Angular profiles in individual $2 \times 2 \times 6$ mm$^3$ qPFG voxel acquired with both $\tau_m = 13.4$ ms and 0 ms were simultaneously fit with the model described above (Eq. (4)) using a Levenberg–Marquardt non-linear least-squares error minimization algorithm to obtain maps of average axon diameters $d$ and intracellular signal fractions $f$. To assess the robustness of our qPFG diffusion MRI methodology in estimating microscopic anisotropy parameters in the presence of orientational mismatch between the applied qPFG diffusion encoding scheme and the underlying anatomy, we conducted an additional control experiment with $\mathbf{q}_1$ and $\mathbf{q}_2$ applied in planes with different orientations with respect to the underlying fiber direction (see Supplementary Material). All calculations were performed in MATLAB and the restricted and free diffusion signals in each sub-voxels were numerically evaluated using the multiple correlation functions framework (*i.e.* Equation 40 in Ozarslan, 2009) and Eq. (3), respectively.

For each subject, regions-of-interest (ROIs) corresponding to the functional specialization of the corpus callosum (Aboitiz et al., 2003) were manually drawn to obtain callosal segments of prefrontal, sensory-motor, temporal/auditory and visual inter-hemispheric white matter fiber bundles. Subsequently, this functional parcellation of the corpus callosum (Huang et al., 2005) was visually validated using full-brain white matter fiber tracking with MEDINRIA (Toussaint et al., 2007). Finally, ROI based analysis was performed for DTI-derived parameters (FA, axial and mean apparent diffusivity) and the estimated average axon diameter and signal volume fraction.

## Results

### Pulse sequence design and implementation

Figs. 4A and B show the diffusion signal attenuation $E^{\mathrm{ax}}(\psi)$ profiles for dPFG and qPFG clinical MRI pulse sequence designs with $TE = 147$ ms and maximum 50 mT/m/axis gradient strength, calculated numerically using our white matter tissue model with a range of axon diameters 1–10 μm and intracellular diffusivity of 1.5 μm$^2$/ms. The parameters for the dPFG pulse sequence were, $G_{max} = 50$ mT/m, $\delta = 22.6$ ms, $\tau_m = 23.4$ ms, $2q = 920$ cm$^{-1}$, and a total b-value of $b = 4610$ s/mm$^2$, while for the qPFG pulse sequence $G_{max} = 50$ mT/m, $\delta = 12.6$ ms, $\tau_m = 13.4$ ms, $4q = 1100$ cm$^{-1}$, and a total b-value of $b = 1200$ s/mm$^2$. As expected based on the analytical solution in Eq. (1), the amplitude of the angular $\psi$-modulation is significantly larger for the qPFG implementation resulting in increased sensitivity to small axon diameters. For example, $\psi$-profiles from 7 μm diameter axons acquired with our qPFG pulse sequence will exhibit a modulation amplitude of 0.21 and an average diffusion signal of 0.56. Meanwhile if the same axon diameter is interrogated using the dPFG pulse sequence, only a 0.11 modulation amplitude can be observed, with 0.33 average diffusion signal (Fig. 4). These results confirm the original findings by Finsterbusch (2010) and suggest that the qPFG diffusion MRI sequence is better suited for clinical use due to its increased sensitivity to small axon diameters and reduced over all diffusion attenuation (b-value).

As our fiber orientation analysis shows in Fig. 2, small misalignments (polar angle $\theta$ and azimuthal angle $\phi$) between the fiber orientation $\hat{\boldsymbol{u}}$ and the normal to the plane of the applied diffusion blocks $\hat{\boldsymbol{n}}$ can cause qualitative changes in the qPFG angular profiles and significantly impact our ability to resolve microscopic anisotropy. As the inclination $\theta$ increases, the coupling between microscopic and macroscopic anisotropy increases generating additional signal minima. For $\phi \neq 90°$, 270° azimuthal deviations decrease the modulation amplitude and shift the peak breaking the symmetry of the $\psi$-profile. These results are in excellent agreement with previous theoretical investigations and highlight the importance of incorporating fiber orientation information in the average axon diameter measurement for clinical mPFG diffusion MRI applications.
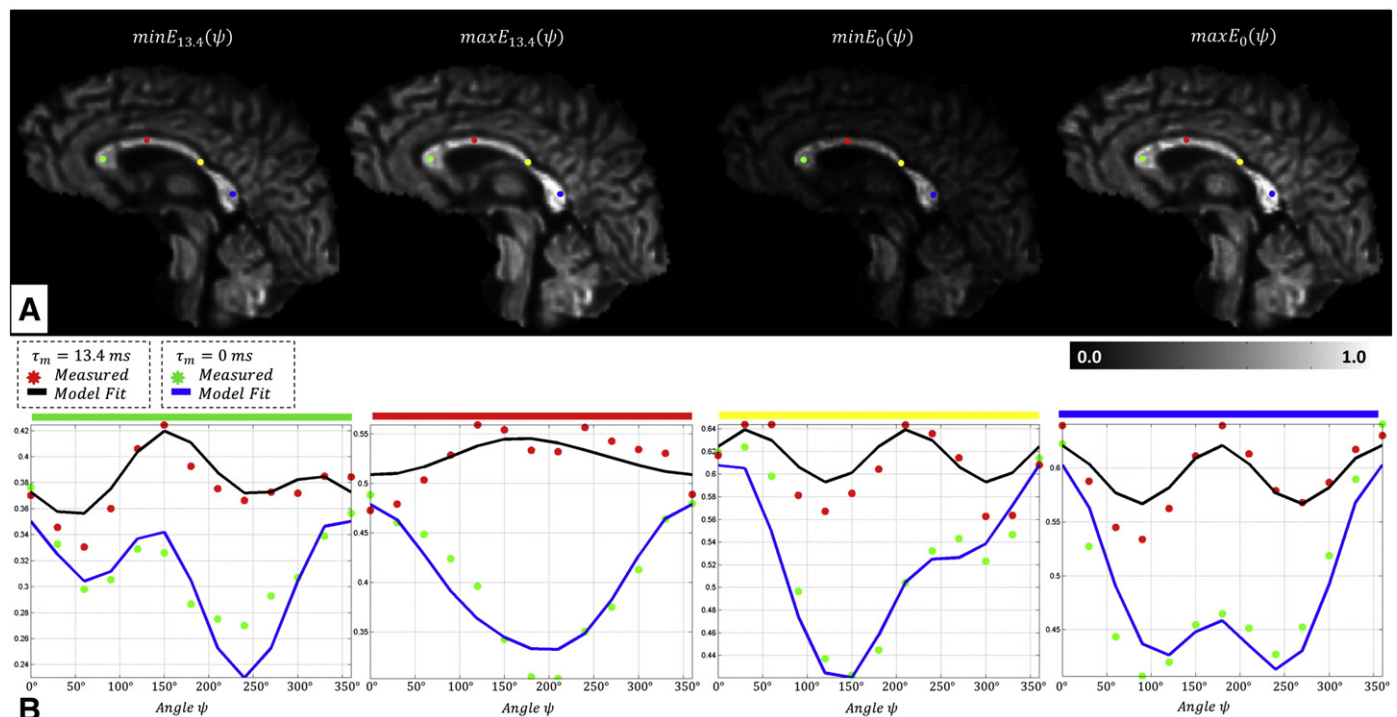


Fig. 6. *In vivo* detection of microscopic anisotropy using quadruple pulsed-field gradient (qPFG) diffusion MRI on a clinical scanner. A. Extrema (minima and maxima) of angular modulation profiles $E_{13.4}(\psi)$ and $E_0(\psi)$ in qPFG diffusion signal attenuation images measured using $\tau_m = 13.4$ ms and $\tau_m = 0.4$ ms, respectively. B. *In vivo* angular qPFG profiles measured in individual voxels in the prefrontal (green), sensory-motor (red), temporal (yellow) and visual (blue) cortical areas show clear signs of restriction-induced microscopic anisotropy. The modulatory effect of imperfect fiber orientation results in features similar to those in Fig. 2. Nevertheless, theoretical angular qPFG profiles generated numerically using Eq. (4) and high-resolution DTI data reveal good agreement with measurements, validating our methodology for isolating microscopic anisotropy information. (For interpretation of the references to color in this figure legend, the reader is referred to the web version of this article.)

*Phantom validation*

Images obtained with our clinical qPFG pulse sequence in the Polyvinylpyrrolidone (PVP) phantom for unrestricted diffusion displayed very good SNR and minimal image distortion due to gradient hardware imperfections (*e.g.*, eddy currents). Single-PFG measurements with *b*-values in the range of 300–3000 s/mm$^2$ resulted in an excellent single-exponential decay fit and a diffusivity of $D_0 = 0.81$ μm$^2$/ms (Fig. 5A), confirming previous results (Pierpaoli et al., 2009). Theoretical angular qPFG diffusion profiles calculated using the diffusivity $D_0$ determined from the single-PFG experiments were in excellent agreement with the empirical $\psi$-profiles measured using our clinical qPFG pulse sequences for $\tau_m = 13.4$ ms and $\tau_m = 0$ ms (Fig. 5B). These results validate the robustness of our numerical methods for quantitatively modeling diffusion experiments conducted using the clinical qPFG diffusion MRI sequences.

*In vivo human data*

Upon validation, the same qPFG MRI technique was used to assess white matter microstructure in healthy human volunteers and to estimate average axon diameters in the corpus callosum. After post-processing using TORTOISE, distortion-corrected registered qPFG DWIs and high-resolution DTI data with good SNR were obtained. Angular profiles similar to those generated numerically (Fig. 2) were measured in individual voxels in the corpus callosum (Fig. 6B). The exclusive effect of microscopic anisotropy could be observed as a positive modulation for measurements with $\tau_m = 13.4$ ms especially in voxels with high fiber coherence. In the case when the diffusion gradient pulses were fused ($\tau_m = 0$ ms), measured angular profiles (Fig. 6B) contained signal contributions from both restricted (intra-axonal) and unrestricted (extracellular) water pools, with the latter resulting in a predominantly negative modulation, similar to that measured in the free diffusion phantom (Fig. 5B). This negative modulation is likely due to an increased signal contribution from extracellular water, which is believed to have a longer $T_2$ relaxation time constant (Whittall et al., 1997). On the other hand, the contribution from any unrestricted water disappears for the measurement with $\tau_m = 13.4$ ms, where the $\psi$-dependence exclusively reflects restriction-induced microscopic anisotropy.

Overall, the diffusion tensor orientations calculated with high-resolution DTI revealed adequate orthogonality between the orientation of the prescribed sagittal slices and the local corpus callosum anatomy (Figs. 3 and 6). Moreover, in slices through the medial corpus callosum, consistency of fiber orientations in the three high-resolution $2 \times 2 \times 2$ mm$^3$ DTI sub-voxels, corresponding to a single $2 \times 2 \times 6$ mm$^3$ qPFG voxel, confirmed good intravoxel fiber coherence (small curvature) supporting the applicability of the impermeable parallel cylinder tissue model for myelinated axons (Assaf and Basser, 2005; Assaf et al., 2008). We focused all subsequent data analysis on the slice through the medial corpus callosum where these conditions were most firmly met.

*Estimating average axon diameters in inter-hemispheric white matter pathways*

For all healthy human volunteers, DTI analysis in the corpus callosum produced standard values of mean apparent diffusion coefficient (ADC) and fractional anisotropy (Table 1). Analysis of residual errors indicated good agreement between fitting results and measured qPFG diffusion data (Fig. 6), especially in regions of high fiber coherence such as the midbody and isthmus of the corpus callosum (*i.e.*, parallel fiber orientations in the corresponding three high-resolution DTI voxels). Maps of trans-callosal average axon diameters indicated significant heterogeneity along the anterior–posterior direction, which was not observable with any DTI-derived metric (Table 1). Moreover, the anterior–posterior organization of axons with different diameters

(Fig. 7E) adequately matched our functionally defined corpus callosum parcellation validated with fiber tracking of white matter pathways connecting brain regions in the prefrontal, sensory-motor, temporal/auditory and visual cortices (Figs. 7D and G). Average axon diameters measured in each of these ROIs (3.85 μm—prefrontal, 6.59 μm—sensory-motor, 4.10 μm—temporal/auditory, and 4.25 μm—visual) are in good agreement with previous post-mortem studies (Aboitiz et al., 1992; Barazany et al., 2009) and support the functional specialization for specific cognitive processing. The intra-axonal signal fractions estimated with qPFG MRI are in line with those reported in the literature (Barazany et al., 2009) and suggest a relatively large contribution from extracellular water signal at the echo time of the diffusion experiment.

## Discussion

Multiple PFG diffusion MRI uniquely characterizes water diffusion caused by microscopic restriction (microscopic anisotropy) providing novel histological information unavailable with conventional DTI. In recent years, numerous studies have validated mPFG MRI theory and methodology in experiments using diverse samples: quartz, emulsions (Shemesh and Cohen, 2011), calibrated glass capillaries (Komlosh et al., 2011), yeast cells (Shemesh et al., 2012), pig spinal cord (Koch and Finsterbusch, 2008; Lawrenz and Finsterbusch, 2011), gray and white matter (Komlosh et al., 2007; Shemesh et al., 2011a). Recently, the possibility of using dPFG diffusion MRI to measure average axon diameters has been demonstrated with histology (Komlosh et al., 2012). Nevertheless, translation of this research from bench to bedside is challenging primarily due to clinical constraints of gradient hardware and scan time.

First, at clinical gradient strengths theoretical assumptions (*e.g.*, $\tau_m \to 0$, $\tau_m \to \infty$, or the short pulse approximation $\delta \to 0$, $\Delta \to \infty$) break down rendering analytical formulas such as Eq. (1) problematic for quantitation of microscopic anisotropy properties. Second, in clinical brain imaging the underlying fiber orientation often deviates from the normal to the ($\mathbf{q_1}$, $\mathbf{q_2}$) plane resulting in strong coupling between microscopic and macroscopic anisotropy, which further complicates the extraction of microscopic anisotropy. Third, the long TE and short scan durations limit the SNR requiring relatively large voxel sizes, which lead to partial volume effects and a broad intravoxel axon size and orientation distributions. Finally, imaging artifacts caused by magnetic field inhomogeneities, bulk and physiological motion, and gradient eddy currents can generate signal confounds and biased estimates of microscopic parameters. While it is possible to acquire mPFG DWIs on whole-body MRI systems (Koch and Finsterbusch, 2011), the extraction of microscopic anisotropy within clinical scan durations requires quantitation of diffusion signals using numerical methods capable of integrating additional information, and a suitable mathematical framework.

A preliminary attempt to adapt dPFG diffusion MRI for clinical scanners was recently reported by Koch and Finsterbusch (2011). Combining pulses on two gradient axes simultaneously to achieve maximum effective gradient strength, the authors of that study acquired dPFG DWIs with $q_1$ and $q_2$ in parallel and antiparallel orientations ($\psi = 0°$, 180°) and statistically estimated a mean pore diameter of 13 μm for axons in a region-of-interest (ROI) along the cortico-spinal tract. These results provide initial evidence supporting the clinical feasibility of dPFG diffusion MRI, but call for improvements in white matter sensitivity and numerical modeling methods. In this study, we designed a novel clinical quadruple PFG diffusion MRI sequence to measure *in vivo* angular profiles over the entire $\psi = 0°$–360° range and analyzed individual voxels using a powerful theoretical framework capable of incorporating high-resolution DTI information (Ozarslan, 2009). Compared to dPFG MRI, our clinical qPFG MRI solution provides improved sensitivity to small axon diameters and reduced diffusional attenuation (Finsterbusch, 2010) allowing robust

**Table 1**

Statistics of DTI- and qPFG MRI-derived parameters across subjects for corpus callosum ROIs corresponding to inter-hemispheric white matter fiber pathways connecting functionally specialized brain regions in the prefrontal (green), sensory-motor (red), temporal/auditory (yellow), and visual (blue) cortices. Estimates for average axon diameters and intra-axonal signal fractions by simultaneously fitting the model to datasets acquired with both $\tau_m = 13.4$ ms and $\tau_m = 0$ ms.

| | Prefrontal | Sensory–motor | Temporal/auditory | Visual |
|---|---|---|---|---|
| Average FA | 0.69 | 0.66 | 0.66 | 0.75 |
| Average ADC ($\mu m^2$ /ms) | 0.71 | 0.73 | 0.76 | 0.68 |
| Intra-axonal signal fraction | 0.36 | 0.30 | 0.41 | 0.35 |
| Average axon diameter ($\mu m$) | 3.85 | 6.59 | 4.10 | 4.25 |

acquisition of high-quality images for quantitative assessment of microscopic anisotropy within scan durations of approximately 15 min. Our results demonstrate the clinical feasibility of quantifying microscopic anisotropy *in vivo* in voxels of a few microliters and show that this information is complementary to parameters derived with conventional DTI (Fig. 7). The topographical correspondence between measured average axon diameter maps and results of previous *ex vivo* studies (Aboitiz et al., 1992; Barazany et al., 2009) provide a preliminary validation for *in vivo* mPFG diffusion MRI and support the clinical potential of this technique.

The possibility of measuring *in vivo* angular qPFG MR signal profiles in good agreement with theoretical calculations confirms the applicability of our model for myelinated axons in white matter. The sagittal prescription through the medial corpus callosum minimizes the number of fibers contributing to the diffusion signal in each voxel thereby restricting the intra-voxel axonal orientation and size distributions. Meanwhile, the large slice thickness generates, even at long TE, adequate SNR for robust qPFG diffusion analysis. Subsequently, high-resolution DTI can be used to better resolve intra-voxel axon orientation distributions improving the quantification of microscopic anisotropy. Unlike single PFG techniques such as AxCaliber, CHARMED or ActiveAx (Alexander et al., 2010), mPFG MRI is inherently more

robust to broad axon diameter distributions (Ozarslan and Basser, 2007). Provided sufficient SNR, measurements with qPFG diffusion encoding applied in planes with different orientations with respect to the underlying microanatomy result in similar estimates of microscopic anisotropy parameters, confirming the robustness of our analysis method (see Supplementary Material). To reduce the complexity of our tissue model we approximate intra- and extracellular diffusivities with apparent axial and mean diffusivities measured with DTI. The intra-axonal diffusivity $D$ has a negligible effect on the angular qPFG profiles generated by human callosal axons with different diameters because, even for small $D$, spins have sufficient time to fully sample 1–10 $\mu m$ compartments during individual diffusion blocks in the proposed clinical qPFG sequences. In comparison, the extracellular diffusivity $D_0$ can affect more sensitively the angular qPFG profile for a given axon diameter, especially when the intra-axonal signal fraction $f$ is small. The accuracy of the estimated microscopic anisotropy metrics could also be affected by limitations of our tissue model such as: diffusion in additional white matter water pools (*e.g.*, oligodendrocytes, capillaries, cerebrospinal fluid) or exchange between restricted and unrestricted water pools. Upon improving the acquisition efficiency and optimizing mPFG diffusion encoding schemes, larger datasets can be acquired and fit with a refined tissue model with additional degrees of freedom (*e.g.* extracellular diffusivity).

Large contributions from extracellular water can decrease the ability of qPFG MRI to discriminate signals from axons with different diameters. In measurements with $\tau_m = 0$ ms, large extracellular signal fractions can generate angular qPFG profiles with negative modulation amplitudes for small caliber axons, and give rise to local extrema in qPFG curves for axons with larger diameters (see Supplementary Material). When datasets with zero and non-zero values of $\tau_m$ are fit simultaneously, the confounding signals from unrestricted extracellular water are qualitatively different (Fig. 5) and can be disentangled more efficiently. The large contribution from free extracellular water to the mPFG signal at $\tau_m = 0$ ms can be mitigated with shorter echo times achieved for example by employing a center-out k-space acquisition or by combining gradients on different axes to increase effective amplitude (Koch and Finsterbusch, 2011).
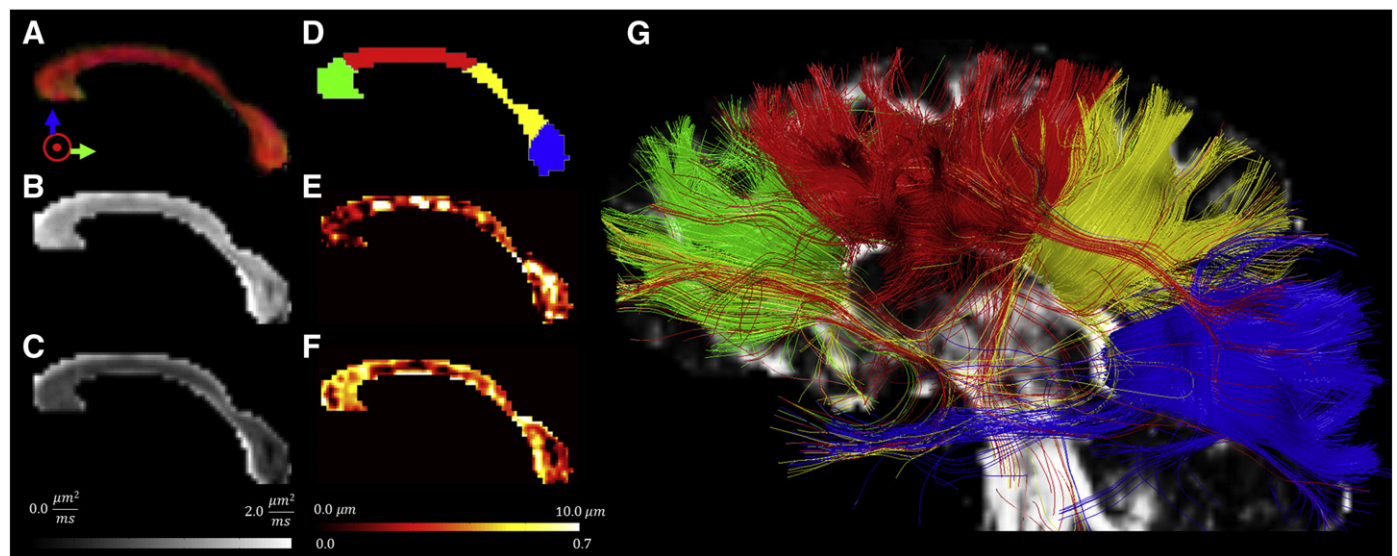


**Fig. 7.** Maps of microstructural information derived with high-resolution diffusion tensor MRI (A,B,C) and quadruple pulsed-field gradient (qPFG) diffusion MRI (E,F) in the corpus callosum of a representative healthy volunteer suggesting that the two methods provide complementary information. A. Direction-encoded color (DEC) map reveals consistent orthogonality between the alignment of callosal fiber pathways and the prescribed sagittal slice orientation. B. Axial diffusivity and C. Mean diffusivity maps show little heterogeneity throughout the corpus callosum. D. Manually drawn regions-of-interest (ROIs) for functional parcellation of the corpus callosum in segments corresponding to prefrontal (green), sensory-motor (red), temporal/auditory (yellow), and visual (blue) inter-hemispheric fiber bundles. E. Map of average axon diameters measured using qPFG diffusion MRI *in vivo* and high-resolution DTI shows significant heterogeneity along the anterior–posterior corpus callosum in good agreement with previous *ex vivo* studies (Aboitiz et al., 2003). F. Corresponding map of intra-axonal signal volume fraction. G. Inter-hemispheric fiber pathways provide a visual validation of the functional parcellation of the corpus callosum. (For interpretation of the references to color in this figure legend, the reader is referred to the web version of this article.)

Sources of imaging artifacts in clinical mPFG MRIs are similar to those encountered in conventional single PFG DWIs, *e.g.*, subject motion, physiological motion, gradient eddy currents, and have been addressed appropriately. Nevertheless, it is important to point out several technical aspects that can affect the accuracy of *in vivo* mPFG MRI measurements. First, gradient eddy currents in mPFG MR with EPI acquisitions can induce $\psi$-dependent image distortions (local image shearing, dilation and compression) resulting in confounding contributions to the angular mPFG diffusion profiles. The use of parallel imaging and/or eddy current distortion correction methods in post-processing can generally mitigate these effects. Second, despite the potential for reducing TE, partial k-space image acquisition strategies should be used with care, as their susceptibility to motion-induced signal loss artifacts can generate inaccurate *in vivo* measurements of microscopic anisotropy. Third, biased quantification of mPFG diffusion profiles could also arise from diffusional contributions of background magnetic field gradients at the microscopic scale, inherent to the sample. Unlike diffusion NMR experiments performed with porous media (Shemesh and Cohen, 2011), clinical diffusion MRI performed at lower field strength on human myelinated axons with diameters of a few micrometers and with moderate variations in tissue magnetic susceptibility should result in negligible diffusional effects (Koch and Finsterbusch, 2011).

Upon further technical refinements and additional clinical validation, the proposed mPFG MRI methodology could find wide clinical applications on present-day MRI systems. It could improve monitoring of normal and abnormal neurodevelopment (*e.g.*, autism) or brain aging in longitudinal studies, provide unique biomarkers for earlier diagnosis of neurodegenerative pathologies (*e.g.* Traumatic Brain Injury), and enable new approaches to structural and functional brain connectivity analysis. Recent advances in high-strength gradient system designs for clinical magnets, such as the Siemens "ConnectomeScanner" (Van Essen et al.) and the growing acceptance of high gradient-strength head-insert coils (Feldman et al., 2011), herald innovative clinical applications of mPFG diffusion MRI leveraging increased SNR, shorter TEs, higher spatial resolution, and more flexibility in varying diffusion encoding parameters (*e.g.*, $\tau_m$, $\Delta$, $\delta$, gradient amplitude, number of mPFGs blocks). Higher gradient amplitude and/or larger number of PFG diffusion blocks for instance could maximize SNR in tissues with larger diffusivities, while increased spatial resolution could resolve partial volume effects and open up the possibility of applying mPFG MRI in convoluted gray matter to quantify small diameter features of randomly oriented dendrites (Komlosh et al., 2007). Finally, mPFG applications are not limited to the human brain. Tissue changes in compartment-specific morphological and microstructural features could be probed in whole-body MRI applications.

## Conclusions

We have established the clinical feasibility of using mPFG diffusion MRI for *in vivo* assessment of microscopic anisotropy on a conventional whole-body MRI scanner. Our results demonstrate that it is possible to detect anisotropy exclusively due to microscopic restrictions using qPFG DWIs acquired with standard gradient hardware within clinically feasible scan durations. The integration of high-resolution DTI and qPFG diffusion MRI data enables extraction of microstructural parameters that uniquely characterize the size of myelinated axons. With impending improvements in gradient hardware technology, mPFG MRI holds the promise of a non-invasive whole brain histological assessment that could prove transformative to neuropathology and neuroimaging.

## Acknowledgments

## Appendix A. Supplementary data

Supplementary data to this article can be found online at http://dx.doi.org/10.1016/j.neuroimage.2012.08.048.

## References

Aboitiz, F., Scheibel, A.B., Fisher, R.S., Zaidel, E., 1992. Fiber composition of the human corpus callosum. Brain Res. 598, 143–153.
Aboitiz, F., Lopez, J., Montiel, J., 2003. Long distance communication in the human brain: timing constraints for inter-hemispheric synchrony and the origin of brain lateralization. Biol. Res. 36, 89–99.
Alexander, D.C., Hubbard, P.L., Hall, M.G., Moore, E.A., Ptito, M., Parker, G.J.M., Dyrby, T.B., 2010. Orientationally invariant indices of axon diameter and density from diffusion MRI. NeuroImage 52, 1374–1389.
Assaf, Y., Basser, P.J., 2005. Composite hindered and restricted model of diffusion (CHARMED) MR imaging of the human brain. NeuroImage 27, 48–58.
Assaf, Y., Blumenfeld-Katzir, T., Yovel, Y., Basser, P.J., 2008. AxCaliber: a method for measuring axon diameter distribution from diffusion MRI. Magn. Reson. Med. 59, 1347–1354.
Barazany, D., Basser, P.J., Assaf, Y., 2009. In vivo measurement of axon diameter distribution in the corpus callosum of rat brain. Brain 132, 1210–1220.
Basser, P.J., 1995. Inferring microstructural features and the physiological state of tissues from diffusion-weighted images. NMR Biomed. 8, 333–344.
Basser, P.J., LeBihan, D., 1994. MR diffusion tensor spectroscopy and imaging. Biophys. J. 66, 259–267.
Basser, P.J., Pajevic, S., Pierpaoli, C., Duda, J., Aldroubi, A., 2000. In vivo fiber tractography using DT-MRI data. Magn. Reson. Med. 44, 625–632.
Beaulieu, C., 2002. The basis of anisotropic water diffusion in the nervous system—a technical review. NMR Biomed. 15, 435–455.
Callaghan, P.T., Eccles, C.D., Xia, Y., 1988. NMR microscopy of dynamic displacements: k-space and q-space imaging. J. Phys. E 21, 820.
Cory, D.G., Garroway, A.N., Miller, J.B., 1990. Applications of spin transport as a probe of local geometry. Polym. Preprints 149.
Feldman, R.E., Scholl, T.J., Alford, J.K., Handler, W.B., Harris, C.T., Chronik, B.A., 2011. Results for diffusion-weighted imaging with a fourth-channel gradient insert. Magn. Reson. Med. 66, 1798–1808.
Finsterbusch, J., 2009. Extension of the double-wave-vector diffusion-weighting experiment to multiple concatenations. J. Magn. Reson. 198, 174–182.
Finsterbusch, J., 2010. Numerical simulations of short-mixing-time double-wave-vector diffusion-weighting experiments with multiple concatenations on whole-body MR systems. J. Magn. Reson. 207, 274–282.
Grebenkov, D.S., 2007. NMR survey of reflected Brownian motion. Rev. Mod. Phys. 79, 1077–1137.
Huang, H., Zhang, J., Jiang, H., Wakana, S., Poetscher, L., Miller, M.I., van Zijl, P.C., Hillis, A.E., Wytik, R., Mori, S., 2005. DTI tractography based parcellation of white matter: application to the mid-sagittal morphology of corpus callosum. NeuroImage 26, 195–205.
Koch, M.A., Finsterbusch, J., 2008. Compartment size estimation with double wave vector diffusion-weighted imaging. Magn. Reson. Med. 60, 90–101.
Koch, M.A., Finsterbusch, J., 2011. Towards compartment size estimation in vivo based on double wave vector diffusion weighting. NMR Biomed. 24, 1422–1432.
Komlosh, M.E., Horkay, F., Freidlin, R.Z., Nevo, U., Assaf, Y., Basser, P.J., 2007. Detection of microscopic anisotropy in gray matter and in a novel tissue phantom using double Pulsed Gradient Spin Echo MR. J. Magn. Reson. 189, 38–45.
Komlosh, M.E., Ozarslan, E., Lizak, M.J., Horkay, F., Schram, V., Shemesh, N., Cohen, Y., Basser, P.J., 2011. Pore diameter mapping using double pulsed-field gradient MRI and its validation using a novel glass capillary array phantom. J. Magn. Reson. 208, 128–135.
Komlosh, M.E., Ozarslan, E., Lizak, M.J., Horkayne-Szakaly, I., Freidlin, R.Z., Basser, P.J., 2012. Average axon diameter mapping of pig spinal cord using d-PFG filtered MRI. ISMRM 20th Annual Meeting, p. 3571. Melbourne, Australia.
Lawrenz, M., Finsterbusch, J., 2011. Detection of microscopic diffusion anisotropy on a whole-body MR system with double wave vector imaging. Magn. Reson. Med. 66, 1405–1415.
Meyer, C.H., Pauly, J.M., Macovski, A., Nishimura, D.G., 1990. Simultaneous spatial and spectral selective excitation. Magn. Reson. Med. 15, 287–304.
Mori, S., Crain, B.J., Chacko, V.P., van Zijl, P.C., 1999. Three-dimensional tracking of axonal projections in the brain by magnetic resonance imaging. Ann. Neurol. 45, 265–269.
Ozarslan, E., 2009. Compartment shape anisotropy (CSA) revealed by double pulsed field gradient MR. J. Magn. Reson. 199, 56–67.
Ozarslan, E., Basser, P.J., 2007. MR diffusion—"diffraction" phenomenon in multi-pulse-field-gradient experiments. J. Magn. Reson. 188, 285–294.

Ozarslan, E., Basser, P.J., 2008. Microscopic anisotropy revealed by NMR double pulsed field gradient experiments with arbitrary timing parameters. J. Chem. Phys. 128, 154511.

Ozarslan, E., Shemesh, N., Basser, P.J., 2009. A general framework to quantify the effect of restricted diffusion on the NMR signal with applications to double pulsed field gradient NMR experiments. J. Chem. Phys. 130, 104702.

Ozarslan, E., Komlosh, M.E., Lizak, M.J., Horkay, F., Basser, P.J., 2011. Double pulsed field gradient (double-PFG) MR imaging (MRI) as a means to measure the size of plant cells. Magn. Reson. Chem. 49, S79–S84.

Pierpaoli, C., Basser, P.J., 1996. Toward a quantitative assessment of diffusion anisotropy. Magn. Reson. Med. 36, 893–906.

Pierpaoli, C., Jezzard, P., Basser, P.J., Barnett, A., Di Chiro, G., 1996. Diffusion tensor MR imaging of the human brain. Radiology 201, 637–648.

Pierpaoli, C., Barnett, A., Pajevic, S., Chen, R., Penix, L.R., Virta, A., Basser, P., 2001. Water diffusion changes in Wallerian degeneration and their dependence on white matter architecture. NeuroImage 13, 1174–1185.

Pierpaoli, C., Sarlls, J., Nevo, U., Basser, P.J., Horkay, F., 2009. Polyvinylpyrrolidone (PVP) water solutions as isotropic phantoms for diffusion MRI studies. ISMRM 17th Annual Meeting, p. 1414. Hawaii, USA.

Pierpaoli, C., Walker, L., Irfanoglu, M.O., Barnett, A., Basser, P., Chang, L.-C., Koay, C., Pajevic, S., Rohde, G., Sarlls, J., Wu, M., 2010. TORTOISE: an integrated software package for processing of diffusion MRI data. ISMRM 18th Annual Meeting, p. 1597. Stockholm, Sweden.

Pruessmann, K.P., Weiger, M., Scheidegger, M.B., Boesiger, P., 1999. SENSE: sensitivity encoding for fast MRI. Magn. Reson. Med. 42, 952–962.

Sarlls, J.E., Pierpaoli, C., Talagala, S.L., Luh, W.-M., 2011. Robust fat suppression at 3T in high-resolution diffusion-weighted single-shot echo-planar imaging of human brain. Magn. Reson. Med. 66, 1658–1665.

Shemesh, N., Cohen, Y., 2011. Overcoming apparent susceptibility-induced anisotropy (aSIA) by bipolar double-pulsed-field-gradient NMR. J. Magn. Reson. 212, 362–369.

Shemesh, N., Barazany, D., Sadan, O., Bar, L., Zur, Y., Barhum, S., Sochen, N., Offen, D., Assaf, Y., Cohen, Y., 2011a. Mapping apparent eccentricity and residual ensemble anisotropy in the gray matter using angular double-pulsed-field-gradient MRI. Magn. Reson. Med. 68, 794–806.

Shemesh, N., Ozarslan, E., Basser, P.J., Cohen, Y., 2011b. Accurate noninvasive measurement of cell size and compartment shape anisotropy in yeast cells using double-pulsed field gradient MR. NMR Biomed. 25, 236–246.

Shemesh, N., Ozarslan, E., Basser, P.J., Cohen, Y., 2012. Accurate noninvasive measurement of cell size and compartment shape anisotropy in yeast cells using double-pulsed field gradient MR. NMR Biomed. 25, 236–246.

Stejskal, E.O., Tanner, J.E., 1965. Spin diffusion measurements: spin echoes in the presence of a time-dependent field gradient. J. Chem. Phys. 42, 288–292.

Toussaint, N., Souplet, J.C., Fillard, P., 2007. MedINRIA: medical imaging navigation and research tool by INRIA. Proc of MICCAI '07 Brisbane, Australia.

Van Essen, D.C., Ugurbil, K., Auerbach, E., Barch, D., Behrens, T.E.J., Bucholz, R., Chang, A., Chen, L., Corbetta, M., Curtiss, S.W., Della Penna, S., Feinberg, D., Glasser, M.F., Harel, N., Heath, A.C., Larson-Prior, L., Marcus, D., Michalareas, G., Moeller, S., Oostenveld, R., Petersen, S.E., Prior, F., Schlaggar, B.L., Smith, S.M., Snyder, A.Z., Xu, J., Yacoub, E., 2012. The human connectome project: a data acquisition perspective. Neuroimage 62, 2222–2231.

Whittall, K.P., Mackay, A.L., Graeb, D.A., Nugent, R.A., Li, D.K.B., Paty, D.W., 1997. In vivo measurement of T2 distributions and water contents in normal human brain. Magn. Reson. Med. 37, 34–43.

Zur, Y., 2000. Design of improved spectral–spatial pulses for routine clinical use. Magn. Reson. Med. 43, 410–420.